This is a repository copy of *In-depth study of intra-Stark spectroscopy in the x-ray range in relativistic laser-plasma interactions*.

Systematic Study of Intra-Stark Spectroscopy in the X-Ray Range in Relativistic Laser-Plasma Interactions

E. Oks,[1] E. Dalimier,[2] A.Ya. Faenov,[3,4] P. Angelo,[2] S.A. Pikuz,[4,5] T.A. Pikuz,[4,6] , I.Yu. Skobelev[4,5], S.N. Ryazanzev[4,7], P. Durey[8], L. Doehl[8], D. Farley[8], C. Baird[8], K.L. Lancaster[8], C.D. Murphy[8], N. Booth,[9] C. Spindloe[9], P. McKenna[10], N. Neumann[11], M. Roth[11], R. Kodama[3,6] and N. Woolsey[8]

[1]*Physics Department, 206 Allison Lab, Auburn University, Auburn, AL 36849, USA*
[2]*LULI - UPMC Univ Paris 06: Sorbonne Universités ; CNRS, Ecole Polytechnique, CEA: Université Paris-Saclay - F-75252 Paris cedex 05, France*
[3]*Open and Transdisciplinary Research Initiative, Osaka University, Suita, Osaka, 565-0871, Japan*
[4]*Joint Institute for High Temperatures, Russian Academy of Sciences, Moscow 125412, Russia*
[5]*National Research Nuclear University MEPhI, Moscow 115409, Russia.*
[6]*PPC and Graduate School of Engineering, Osaka University, 2-1, Yamadaoka, Suita, Osaka 565-0871, Japan*
[7]*Moscow State University, Moscow, 119991, Russia*
[8]*York Plasma Institute, Department of Physics, University of York, York YO10 5DD, UK*
[9]*Central Laser Facility, STFC Rutherford Appleton Laboratory, Didcot OX11 0QX, UK*
[10]*Department of Physics, SUPA, University of Strathclyde, Glasgow G4 0NG, UK*

[11]*Institut fur Kernphysik, Technische Univesitat Darmstadt, Schlossgartenstraße 9, 64289 Darmstadt, Germany*

Corresponding authors emails: goks@physics.auburn.edu, faenov.anatoly@photon.osaka-u.ac.jp

Abstract

Intra-Stark Spectroscopy (ISS) is the spectroscopy within the quasistatic Stark profile of a spectral line. In the ISS some local depressions ('dips') occur at certain locations of the quasistatic Stark profile of a spectral line. This phenomenon arises when radiating atoms/ions are subjected simultaneously to a quasistatic field $\mathbf{F}$ and to a quasimonochromatic electric field $\mathbf{E}(t)$ at the characteristic frequency ω. The present paper advances the study of the relativistic laser-plasma interaction from our previous paper (Oks et al, Optics Express **25** (2017) 1958). First, by improving the experimental conditions and the diagnostics, it provides a *systematic* spectroscopic study of the simultaneous production of the Langmuir waves and of the ion acoustic turbulence at the surface of the relativistic critical density. It demonstrates a reliable reproducibility of the Langmuir-wave-induced dips at the same locations in the experimental profiles of Si XIV Ly-beta line, as well as of the deduced parameters (fields) of the Langmuir waves and ion acoustic turbulence in different laser shots. Second, this study employs for the first time *the most rigorous condition of the dynamic resonance*, on which the ISS phenomenon is based, compared to all previous studies in all kinds of plasmas in a wide range of electron densities. It shows how different interplays between the Langmuir wave field and the field of the ion acoustic turbulence lead to distinct spectral line profiles, including the disappearance of the Langmuir-wave-induced dips.

Keywords: intra-Stark spectroscopy, relativistic laser-plasma interaction, x-ray spectral line profiles, parametric decay instability

1. Introduction

Plasma spectroscopy provides powerful tools for diagnostics of various laboratory and astrophysical plasmas – see, for example, books [1-8] published over the last 25 years and listed in the chronological order. An important part of plasma spectroscopy is the Intra-Stark Spectroscopy (ISS), which is the spectroscopy within the quasistatic Stark profile of a spectral line. This terminology was introduced first in papers [9, 10] because of some physical analogy with the well-known Intra-Doppler Spectroscopy, where due to nonlinear optical phenomena some depressions occur at certain locations of the Doppler profile of a spectral line. In the ISS some local depressions ('dips') occur at certain locations of the quasistatic Stark profile of a spectral line. This phenomenon arises when radiating atoms/ions are subjected simultaneously to a quasistatic field $\mathbf{F}$ and to a quasimonochromatic electric field $\mathbf{E}(t)$ at the characteristic frequency ω. In the heart of this phenomenon is the dynamic resonance between the Stark splitting of hydrogenic spectral lines and the frequency ω or its harmonics. The greatest distinction of ISS from Intra-Doppler Spectroscopy is that in ISS, despite the applied electric field being quasimonochromatic, there occurs a nonlinear dynamic resonance of a multifrequency nature, as explained in detail in paper [11]. Further details on the theory of the ISS can be found in book [1].

The most studied experimentally is the situation where the quasimonochromatic electric field $\mathbf{E}(t)$ represents a Langmuir wave. The corresponding dips in spectral line profiles are called L-dips. The practical significance of studies of the L-dips is threefold. First, they provide the most accurate passive spectroscopic method for measuring the electron density N_e in plasmas, e.g. more accurate than line broadening measurements. In the benchmark experiment of Kunze's group [10], where plasma parameters were measured independently of spectral line shapes, it was shown that this passive spectroscopic method for measuring N_e does not differ in its high accuracy from the active spectroscopic method – more complicated experimentally – using the Thompson scattering. Second, they provide the only non-perturbative method for measuring the amplitude of Langmuir waves in plasmas. Third, in laser-produced plasmas they help to reveal the physics of the laser-plasma interaction.

Book [1] and later reviews [12-14] summarize all the experimental studies of the L-dips with applications to plasma diagnostics. Specifically, in x-ray spectral line profiles emitted in laser-plasma interactions, there were three experimental studies (and diagnostic applications) of the ISS, as follows.*/

In the first study, reported in paper [16], the incident laser intensity was relatively low: 2×10^{14} W/cm^2. In the second study, reported in paper [17], where the experiment was performed using a femtosecond laser-driven cluster-based plasma, the incident laser intensity was $(0.4 - 3) \times 10^{18}$ W/cm^2 (on the threshold for relativistic laser plasma interaction). In the third study, reported in

----

*/ We note also the experimental study of the L-dips in x-ray spectral line profiles performed at the Z-pinch [15] rather than in laser-produced plasmas.

paper [18], the incident laser intensity was ~10^{21} W/cm^2, causing strongly relativistic laser-plasma interaction. In the latter experiment, in addition to the Langmuir waves, there were discovered spectroscopically, for the first time, *ion acoustic waves* in laser-produced, high-density plasmas; the simultaneous production of both kinds of these waves was attributed to the development of the Parametric Decay Instability (PDI) [19] at the surface of the *relativistic* critical density.

The work reported in the present paper advances the study of the relativistic laser-plasma interactions from paper [18] by having the following new features. First, in the present experiment a plasma mirror was used to significantly improve the laser contrast. As a result, there was a much smaller laser pre-plasma (compared to the experiment from paper [18]), allowing the main laser pulse to interact with a higher density plasma.

Second, this improvement enabled us to perform a *systematic* spectroscopic study of the simultaneous production of the Langmuir waves and of the ion acoustic turbulence at the surface of the relativistic critical density. This was achieved by the spectroscopic analysis of the same spectral line (Si XIV Ly-beta) in three different shots of about the same laser intensity 2×10^{20} W/cm^2. This demonstrated reliable reproducibility of the L-dips at the same locations in the experimental profiles, as well as of the deduced parameters (fields) of the Langmuir waves and ion acoustic turbulence in all three shots.

Third, this study employed for the first time *the most rigorous condition of the dynamic resonance* (which makes possible the ISS phenomenon) compared to all previous studies in all kinds of plasmas, over a wide range of electron densities. By doing so we showed how different interplays between the Langmuir wave field with the field of the ion acoustic turbulence lead to distinct spectral line profiles, including the disappearance of the L-dips.

2. X-ray spectra measurements

The experiments were performed at Vulcan Petawatt (PW) laser facility at the Rutherford Appleton Laboratory [20]. Vulcan PW generates a beam using optical parametric, chirped pulse amplification (OPCPA) technology at central wavelength of 1054 nm and a pulse of the duration at the full-width-half-maximum (FWHM) of ~1.0 ps. In our previous experiments [18], the OPCPA technology was used, enabling an amplified spontaneous emission (ASE) to the peak-intensity contrast ratio exceeding 10^{-9}. In our present experiments a plasma mirror [21] was employed to increase the contrast ratio to the 10^{-11} range, ensuring that the main pulse interacted with an unperturbed, cold target. The highest laser pulse energy measured before the compressor was ~620 J, while the efficiency of the beam delivery line including the laser compressor, f/3 off-axis parabolic mirror and plasma mirror was measured as 50%, which corresponds to ~300 J laser energy on target on average. The p-polarized, focusing beam was reflected by the plasma mirror, to a focal spot of 7 μm (FWHM), at an incident angle of 45° to the normal to the target surface, as shown in Fig.1. The central focal spot contained 30% of the laser energy, resulting in a maximum intensity of ~2-3×10^{20} W/cm^2.

The x-ray emission of the plasma was registered by means of a focusing spectrometer, with a spatial resolution (FSSR), at the directions close to the normal to the target surface, from the rear side of the target. To obtain the spectra with a high spectral resolution ($\lambda/\delta\lambda \sim 3000$) in a rather broad range from 5.15 to 5.85 Å, the FSSR [22-24] was equipped with quartz spherically bent (radius of curvature R=150 mm) crystal 10-11 (2d ~ 6.6 A) installed at a distance of 332 mm from the target.

The spectra were recorded by means of Fujfilm TR Image Plate (IP) detectors protected against the exposure to the visible light by two layers of 1 µm-thick polypropylene $(C_3H_6)_n$ with 0.2 µm Al coating. Additionally, to prevent saturation of the detectors, the Mylar $(C_{10}H_8O_4)$ filter of 5 µm thickness was placed at the magnet entrance. The background fogging and crystal fluorescence due to intense fast electrons was limited by using a pair of 0.5 T neodymium-iron-boron permanent magnets that formed a 10 mm wide slit in front of each crystal. Typical K-shell X-ray spectra of Si measured from the rear side of different solid targets are presented in Fig. 1(b).
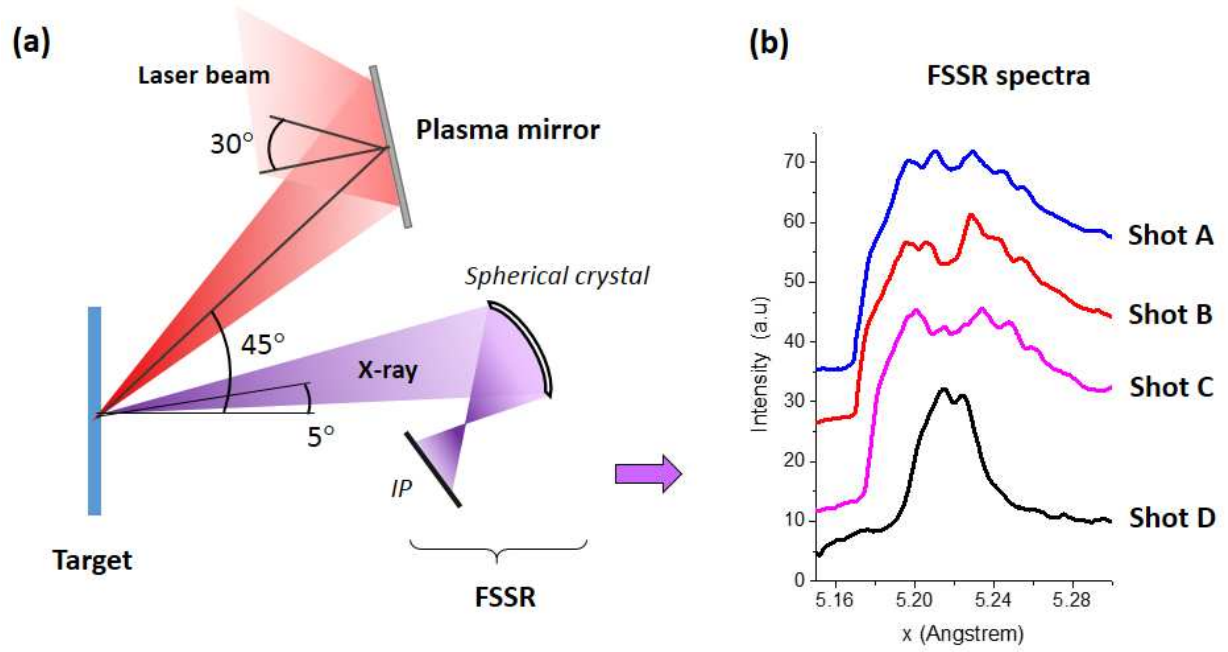
Fig. 1. (a) Schematic of the experimental setup. (b) High resolution spectral measurements of the Ly$_\beta$ line of Si XIV obtained in different laser shots (see Table 1 for details of the laser shot parameters).

Four types of targets were used in our experiment. The parameters of the targets and laser pulses are presented in Table 1.

Table 1. Target and laser shot parameters used in the present experiments

Target/ Shot	Laser energy, J	Laser energy on target, J	Laser pulse length, ps	Focal spot diameter, µm	Intensity on the target, 10^{20} W/cm^2
Si 2 um/ Shot A	620 (+/- 10%)	310	1.2	7	2.0
CH 2um + Si 2um + CH 2 um/Shot B	490 (+/- 10%)	245	1	7	1.9

CH 2 μm + Si 2 μm/Shot C	520 (+/- 10%)	260	1.1	7	1.9
Si3N4 0.5 um/Shot D	225(+/- 10%)	110	1	7	0.9

3. Analysis of the experimental profiles of the Si XIV Ly-beta line

In shots A,B,C, the experimental profiles, indicated by "Exp" in Fig. 2, exhibit two very distinct bump-dip-bump structures. The dips are located practically symmetrically with respect to the unperturbed wavelength of the line: one dip – in the blue wing, the other – in the red wing. Below we present the evidence that these are Langmuir-wave-induced dips (L-dips). Moreover, each of them is an L-super-dip, i.e., the superposition of two L-dips at the same location.
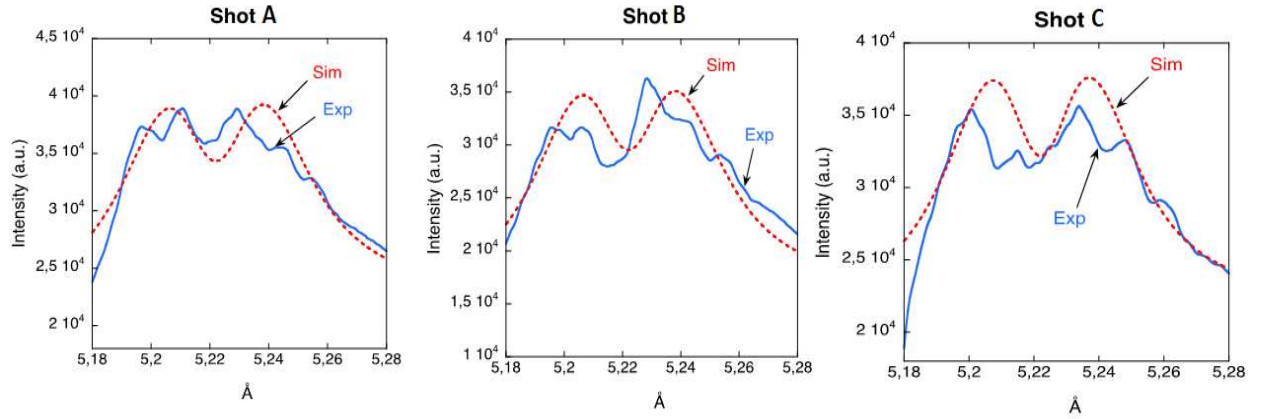

Fig. 2. Experimental profiles of the Si XIV Ly-beta line in shots A,B,C (blue color in the online version) and their comparison with simulations using code FLYCHK (red color in the online version) at the electron density $N_e = 6 \times 10^{23}$ cm^{-3} and the temperature T = 500 eV.

According to the theory [1], L-dips originate from a dynamic resonance between the Stark splitting

$$\omega_{stark}(F) = 3n\hbar F/(2Z_r m_e e) \tag{1}$$

of hydrogenic energy levels, caused by a quasistatic field **F** in a plasma, and the frequency ω_L of the Langmuir wave, which practically coincides with the plasma electron frequency $\omega_{pe} = (4\pi e^2 N_e/m_e)^{1/2}$:

$$\omega_{stark}(F) = s\omega_{pe}(N_e), \quad s = 1, 2, \ldots \tag{2}$$

Here n and Z_r are the principal quantum number and the nuclear charge of the radiating hydrogenic atom/ion (radiator), s is the number of quanta (Langmuir plasmons) involved in the resonance.

From the resonance condition (2), one determines specific locations of L-dips in spectral line profiles, which depend on N_e, since ω_{pe} depends on N_e. In particular, in the situation where the quasistatic field **F** is dominated by the Low-frequency Electrostatic Turbulence (LET), e.g., the ion acoustic turbulence, for the Ly-lines, the distance of an L-dip from the unperturbed wavelength λ_0 can be expressed as: $\Delta\lambda_{dip}(qs, N_e) = \left[\lambda_0^2 / (2\pi c)\right] qs\omega_{pe}(N_e)$. Here $q = n_1 - n_2$ is the electric quantum number expressed via the parabolic quantum numbers n_1 and n_2: $q = 0, \pm1, \pm2, ..., \pm(n-1)$. The electric quantum number marks Stark components of Ly-lines. For a pair of Stark components, corresponding to the electric quantum numbers q and $-q$, there could be a pair of L-dips located symmetrically in the red and blue parts of the spectral line profile:

$$\Delta\lambda_{dip}(qs, N_e) = \pm\left[\lambda_0^2 / (2\pi c)\right] qs\omega_{pe}(N_e). \qquad (3)$$

Equation (3) shows that for a given electron density N_e, the location of the pair of L-dips is controlled by the product $|q|s$.

The Ly-beta line has two Stark components in each wing, corresponding to $q = 1$ and $q = 2$. Therefore, the L-dip in the profile of the component of $q = 1$ due to the two-quantum resonance ($s = 2$) coincides by its location with the L-dip in the profile of the component of $q = 2$ due to the one-quantum resonance ($s = 1$). The superposition of two different L-dips at the same location results in the L-super-dip with significantly enhanced visibility.

This L-super-dip is observed twice in the experimental profiles of the Si XIV Ly-beta line in shots A,B,and C: one − in the blue part and the other in the red part. These L-super-dips are located practically symmetrically at the distance $\Delta\lambda_{dip}(N_e) = 24$ mA from the unperturbed wavelength. According to Eq. (3) with $|q|s = 2$, this translates into the electron density $N_e = 2.2\times10^{22}$ cm^{-3} (We remind the reader that this passive spectroscopic method for measuring N_e is just as accurate as the active spectroscopic method using the Thompson scattering, as noted in the Introduction, with the reference to the benchmark experiment [10]). This electron density is about the same as deduced in paper [25] by analyzing total intensities (rather than shapes) of Si XIV and Si XIII spectral lines (using code ATOMIC) in the plasma region (called zone 1 in [25]), from which these lines were emitted, the experiment being performed at the same laser facility at about the same incident laser intensities.

As for the would-be L-dip corresponding to $|q|s = 1$, i.e., the L-dip in the profile of the Stark component of $q=1$ due to the one-quantum resonance ($s = 1$), it is not visible in the experimental profiles for the following reason. The location, where this L-dip would have been occurred, is too close to the central part of the profile. The central part of the profile correspond to the relatively small values of the field F, which are not quasistatic – see, for example, review [26]. Therefore, the would-be L-dips, corresponding to $|q|s = 1$ would not be observed.

At the absence of the LET, the quasistatic field required for the formation of the L-dips would be represented by the ion microfield. In this case, for relatively high electron densities, such as $N_e > 10^{22}$ cm^{-3}, due to the spatial non-uniformity of the ion microfield the mid-point between the two L-dips in the pair would be significantly red-shifted [10, 1]. However, such shift was not observed in the present experiment. This is an indication that the quasistatic field required for the formation of the L-dips was represented primarily by the LET dominating the ion microfield.

Another indication of the presence of the LET comes from modeling the experimental profile using the code FLYCHK. This is an advanced code, but it does not take into account of the LET and the L-dips (the modelled profiles are shown in Fig. 2). It yielded T = 500 eV and $N_e = 6\times10^{23}$

cm^{-3}. This value of N_e is one and a half orders of magnitude higher than the electron density $N_e = 2.2 \times 10^{22}$ cm^{-3} deduced from the experimental L-dips.

The physical mechanism producing simultaneously the Langmuir waves and the LET (specifically, the ion acoustic turbulence) out of the laser field is the Parametric Decay Instability (PDI). PDI is a nonlinear process, in which an electromagnetic wave decays into a Langmuir wave and an ion acoustic wave at the surface of the critical density N_c determined from the equation

$$\omega = \omega_{pe}(N_c), \tag{4}$$

where ω is the laser frequency – see e.g. references [19, 27]. For the laser frequency ω corresponding to the wavelength λ of approximately 1054 nm in the present experiment, Eq. (4) yields $N_c = 1.0 \times 10^{21}$ cm^{-3}. However, for relativistic laser intensities $I > 10^{18}$ W/cm^2, i.e. those corresponding to the present experiment, the 'relativistic' critical electron density N_{cr} becomes greater than N_c [28-30]. For the linearly-polarized laser radiation, it becomes [31]

$$N_{cr} = \frac{(\pi a/4)m_e\omega^2}{4\pi e^2}, \qquad a = \lambda(\mu m)\left[\frac{I(W/cm^2)}{1.37 x 10^{18}}\right]^{1/2} \tag{5}$$

For the laser intensities of the incident laser wave *at the surface of the target I_{surf}* = 2×10^{20} W/cm^2, used in shots A,B and C Eq. (5) yields $N_{cr} = 1 \times 10^{22}$ cm^{-3}, which is just a factor of two smaller than the electron density $N_e = 2.2 \times 10^{22}$ cm^{-3} deduced from the experimental L-dips.

However, the actual intensity of the transverse electromagnetic wave in the plasma can be significantly greater than the intensity of the incident laser radiation at the surface of the target because of a number of physical effects. One of them is the self-focusing of the laser beam in plasmas – see, e.g., papers [32, 33] and reviews [34, 35) providing details of the process of the laser propagation in the plasma corona at the overcritical density. The other relevant effects enhancing the transverse electromagnetic wave in the plasma are Raman and Brillouin backscattering. There are experimental proofs of such enhancement – see. e.g., paper [36]. In the present experiment in shots A, B and C, for the relativistic critical density to be approximately equal to the density $N_e = 2.2 \times 10^{22}$ cm^{-3} deduced by the spectroscopic analysis, would require only a factor of two enhancement in the laser amplitude.

Thus, it was the PDI at the surface of the relativistic critical density that produced simultaneously the Langmuir waves and the ion acoustic turbulence in shots A,B and C. The amplitude E_0 of the Langmuir wave can be determined immediately from the experimental profile by using the expression for the half-width $\delta\lambda_{1/2}$ of the L-dip, i.e., the separation between the dip and the nearest "bump" [1]:

$$\Delta\lambda_{1/2} = (3/2)^{1/2}\lambda_0^2 n^2 \hbar E_0/(8\pi m_e e c Z_r). \tag{6}$$

Substituting the experimental $\delta\lambda_{1/2}$ in Eq. (6), we obtain the following values of the amplitude of the Langmuir waves: E_0 = 0.7 GV/cm, 0.5 GV/cm, and 0.6 GV/cm for shots A, B and C, respectively.

The resonant value of the quasistatic field F_{res} responsible for the formation of the L-dips, can be determined from the resonance condition (1):

$$\omega_{stark}(F_{res}) = s\omega_{pe}(N_e). \tag{7}$$

For the formation of the L-dips the value of F_{res} is required to be at least several times higher than E_0 (the L-dips cannot form if $E_0/F_{res} > 0.5$) – see [1]. For shots A, B and C, Eq. (7) yields: $F_{res} = 6.5$ GV/cm for $s = 2$ and $F_{res} = 3.25$ GV/cm for $s = 1$. These values of F_{res} are about 10 and 5 times higher than the Langmuir wave amplitude E_0, respectively. Thus, the condition necessary for the formation of the L-dips was fulfilled in shots A, B and C   For a detailed quantitative analysis/modeling, we calculated the theoretical profiles, providing the best fit to the experimental profiles from shots A, B and C as follows. The total quasistatic field **F** is the vector sum of two contributions: $\mathbf{F} = \mathbf{F_t} + \mathbf{F_i}$. The first contribution $\mathbf{F_t}$ is the field of a LET, while the second contribution $\mathbf{F_i}$ is the quasistatic part of the ion microfield. We employed the results from paper [37] to calculate the distributions of the total quasistatic field $\mathbf{F} = \mathbf{F_t} + \mathbf{F_i}$,. Specifically, we calculated the distribution of the total quasistatic field **F** in the form of the convolution of the APEX distribution of $\mathbf{F}_i$ [38] with the Rayleigh-type distribution of $\mathbf{F}_t$ [37] (We note that for the case where the characteristic value of the LET is much greater than the characteristic value of the ion microfield, the analytical results from paper [39] provide a robust way to calculate the distribution of the total quasistatic field without calculating the convolution, though we did not use these results here). We also took into account the broadening by the electron microfield, the Doppler, the instrumental broadenings, as well as the theoretically expected asymmetry of the profiles (for the theory of the asymmetry we could refer to papers [40, 41] and references therein). For calculating the details of the spectral line shape in the regions of L-dips we employed the analytical solution in references [11, 1] for the wave functions of the quasienergy states, the latter being caused simultaneously by all harmonics of the total electric field $\mathbf{E}(t) = \mathbf{F} + \mathbf{E}_0 \cos(\omega_{pe}t)$ (vectors **F** and $\mathbf{E}_0$ are not collinear). For additional details we refer to paper [11] and to book [1] (Sect. 4.2).

Figure 3 shows the comparison of the theoretical profiles, allowing, in particular, for the LET and L-dips, with the corresponding experimental profiles from shots A, B and C. The theoretical profiles were calculated at $N_e = 2.2\times10^{22}$ cm^{-3} and the temperature $T = 600$ eV, 550 eV, and 600 eV for shots 18, 22, and 24, respectively. The comparison demonstrates good agreement between the theoretical and experimental profiles, and thus reinforces our interpretation of the experimental profiles.

This modeling yielded the following values of the root-mean-square field of the LET: $F_{t,rms} = 4.8$ GV/cm, 4.4 GV/cm, and 4.9 GV/cm for shots A, B and C respectively. For comparison, the characteristic ion microfield $F_{i,typ} = 2.603 \, eZ^{1/3}N_e^{2/3}$ was 1.5 GV/cm.
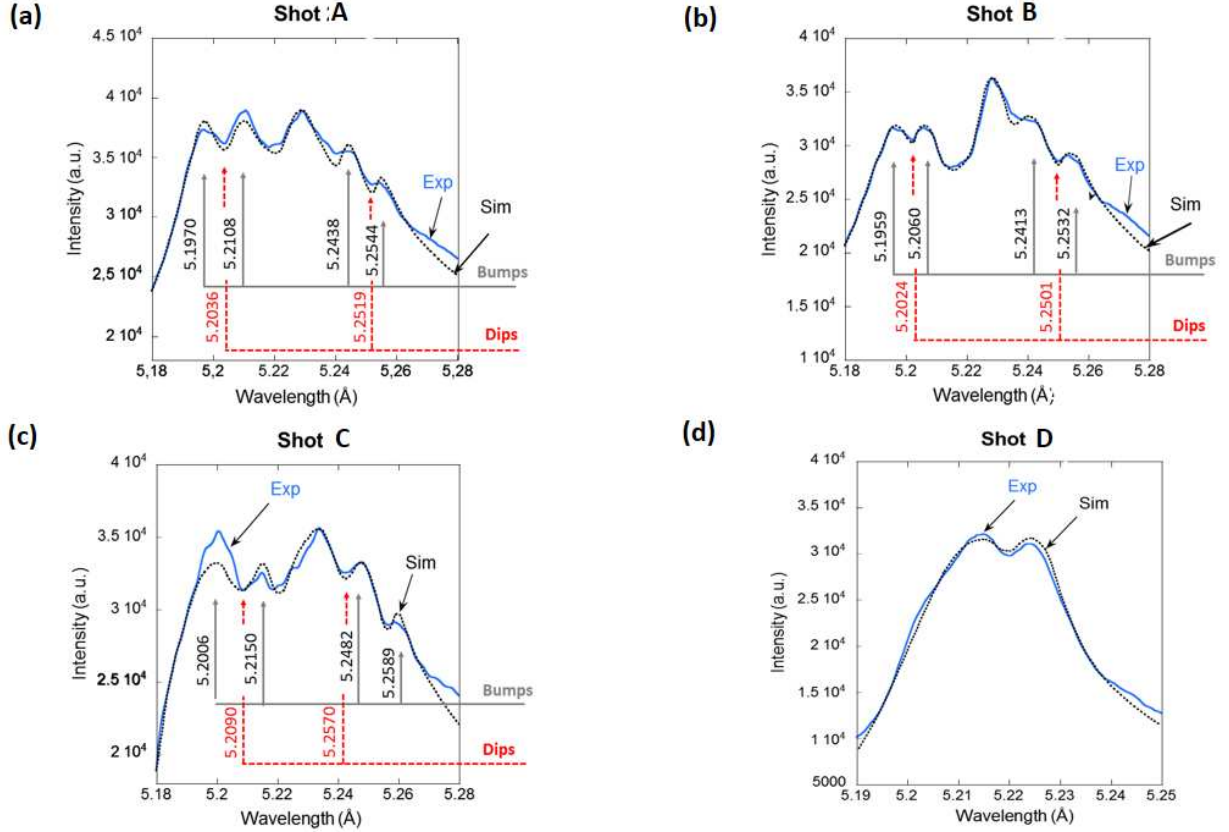
Fig. 3. Comparison of the experimental profiles of the Si XIV Ly-beta line (solid line, blue in the online version, marked Exp) with the theoretical profiles (dotted line, black, marked Sim) allowing for the effects of the Langmuir waves, the LET, and all other broadening mechanisms (see the text). In the profiles from shots A, B and C, there are clearly seen 'bump-dip-bump' structures (both in the red and blue parts of the profiles) typical for the L-dips phenomenon. The following parameters provided the best fit: (a) $N_e = 2.2\times10^{22}$ cm^{-3}, $T = 600$ eV, $F_{t,rms} = 4.8$ GV/cm, $E_0 = 0.7$ GV/cm; (b) $N_e = 2.2\times10^{22}$ cm^{-3}, $T = 550$ eV, $F_{t,rms} = 4.4$ GV/cm, $E_0 = 0.5$ GV/cm; (c) $N_e = 2.2\times10^{22}$ cm^{-3}, $T = 600$ eV, $F_{t,rms} = 4.9$ GV/cm, $E_0 = 0.6$ GV/cm; (d) $N_e = 6.6\times10^{21}$ cm^{-3}, $T = 550$ eV, $F_{t,rms} = 2.0$ GV/cm, $E_0 = 2.0$ GV/cm.

Now we proceed to analyze the experimental profile of the Si XIV Ly-beta line in shot D - see Fig. 3 (d). The experimental profile does not show bump-dip-bump structures – in distinction to shots A, B and C. In shot D the incident laser intensity was $I = 8.8\times10^{19}$ W/cm^2, i.e., it was significantly lower than in shots A, B and C. The corresponding relativistic critical density is $N_e = 6.6\times10^{21}$ cm^{-3}. The modeling using code FLYCHK (that does not take into account the LET and the Langmuir waves) yielded $N_e = 1.7\times10^{23}$ cm^{-3}, which is one and a half orders of magnitude higher than the relativistic critical density.

It is unlikely that the experimental profile in shot D, produced at the significantly smaller laser intensity than in shots A, B and C, would be emitted from the region of the electron density $N_e = 1.7\times10^{23}$ cm^{-3} by an order of magnitude higher than the region of the electron density $N_e = 2.2\times10^{22}$ cm^{-3}, from which the experimental profiles were emitted in shots A, B and C. The most probable interpretation of the experimental profile in shot D is the following.

In shot D the electron density was significantly lower than in shots A, B and C. Therefore the damping of the Langmuir waves was significantly lower, which could allow the Langmuir waves

to reach a significantly higher amplitude. Figure 3(d) shows the comparison of the experimental profile from shot D with the modeling based on the code allowing for the LET and the Langmuir waves at $N_e = 6.6 \times 10^{21}$ cm^{-3}, $T = 550$ eV, $F_{t,rms} = 2.0$ GV/cm, $E_0 = 2.0$ GV/cm. It is seen that this theoretical profile is in a good agreement with the experimental profile and it does not exhibit bump-dip-bump structures. Here is the reason why.

When the ratio $E_0/F_{res} > 0.5$, the L-dips cannot form – as mentioned above with the reference to book [1]. The determination of the resonant value F_{res} of the quasistatic field from Eq. (7) is valid only for $E_0 << F_{res}$. For being valid for arbitrary ratios of E_o to F_{res}, Eq. (7) should be modified as follows (according to book [1]):

$$\omega_{stark}(F_{res})\, g(\varepsilon) = s\omega_{pe}\,(N_e), \quad g(\varepsilon) = (1 + \varepsilon^2)^{1/2}\, \text{EllipticE}[\varepsilon/(1 + \varepsilon^2)^{1/2}], \qquad \varepsilon = E_o/F_{res}, \qquad (8)$$

where $\omega_{stark}(F_{res})$ is still given by Eq. (1) and EllipticE[…] is the complete elliptic integral of the 2nd kind. For $N_e = 6.6 \times 10^{21}$ cm^{-3} and $E_0 = 2.0$ GV/cm, Eq. (8) yields $F_{res} = 1.7$ GV/cm for $s = 1$ (so that $E_o/F_{res} = 1.2$) and $F_{res} = 3.5$ GV/cm for $s = 2$ (so that $E_o/F_{res} = 0.6$). Thus, both for the one-quantum resonance ($s = 1$) and for the two-quantum resonance ($s = 2$), we get $E_0/F_{res} > 0.5$, so that the L-dips were not able to form. So, most probably in shot D the PDI did occur at the surface of the relativistic critical density, resulting in the development of both the Langmuir waves and the ion acoustic turbulence, but without producing the L-dips in the experimental line profile. We note that, while for shots A, B and C the electron density was unequivocally deduced simply from the locations of the L-dips, in shot D it turned out possible to deduce the electron density by modeling the entire experimental profile using the code that allows for the interplay of the LET and the Langmuir waves.

4. Conclusions

We performed a systematic spectroscopic study of the simultaneous production of Langmuir waves and of the ion acoustic turbulence at the surface of the relativistic critical density under the relativistic laser-plasma interaction. We demonstrated a reliable reproducibility of the L-dips at the same locations in the experimental profiles, as well as of the deduced parameters (fields) of the Langmuir waves and ion acoustic turbulence. By doing so, we expanded applications of the intra-Stark spectroscopy and reinforced the validity of the physics behind these different waves as being caused by the parametric decay instability at the surface of the relativistic critical density.

We also employed, for the first time, the most rigorous condition of the dynamic resonance, on which the intra-Stark spectroscopy is based, compared to all previous studies in all kinds of plasmas in a wide range of electron densities. As a result, we were able to show how different interplay between the Langmuir wave field with the field of the ion acoustic turbulence lead to distinct manifestations in the spectral line profiles, including the disappearance of the L-dips.

We hope that our results will motivate further applications of the intra-Stark spectroscopy to studies of laser-produced plasmas in general, and to studies of relativistic laser-plasma interactions in particular.

References

1. E. Oks, *Plasma Spectroscopy: The Influence of Microwave and Laser Fields*, Springer

Series on Atoms and Plasmas, vol. 9 (Springer, New York) 1995

2. H.R. Griem, *Principles of Plasma Spectroscopy* (Cambridge University Press, Cambridge) 1997

3. D. Salzman, *Atomic Physics in Hot Plasmas* (Oxford University Press, Oxford) 1998

4. T. Fujimoto, *Plasma Spectroscopy*(Clarendon Press, Oxford, UK) 2004

5. I.H. Hutchinson, *Principles of Plasma Diagnostics* (Cambridge University Press, Cambridge) 2005

6. E. Oks, *Stark Broadening of Hydrogen and Hydrogenlike Spectral Lines in Plasmas: The Physical Insight* (Alpha Science International, Oxford, UK) 2006.

7. H.-J. Kunze, *Introduction to Plasma Spectroscopy* (Springer, Berlin) 2009.

8. E. Oks, *Diagnostics of Laboratory and Astrophysical Plasmas Using Spectral Lines of One-, Two-, and Three-Electron Systems* (World Scientific, New Jersey) 2017

9. V.P. Gavrilenko and E. Oks, Sov. Phys. J. Plasma Phys. **13** (1987) 22

10. E. Oks, St. Böddeker, and H.-J. Kunze, Phys. Rev. A **44** (1991) 8338

11. V.P. Gavrilenko and E. Oks, Sov. Phys. JETP **53** (1981) 1122

12. E. Dalimier, E. Oks, and O. Renner, Atoms **2** (2014) 178

13. E. Dalimier, A. Ya Faenov, E. Oks, P. Angelo, T.A. Pikuz, Y. Fukuda, A. Andreev, J. Koga, H. Sakaki, H. Kotaki, A. Pirozhkov, Y. Hayashi, I.Yu. Skobelev, S.A. Pikuz, T. Kawachi, M. Kando, K. Kondo, A. Zhidkov, E. Tubman, N.M.H. Butler, R.J. Dance, M.A. Alkhimova, N. Booth, J. Green, C. Gregory, P. McKenna, N. Woolsey, and R. Kodama, J. Phys. Conf. Ser. **810** (2017) 012004

14. E. Dalimier, E. Oks, and O. Renner, AIP Conference Proceedings **1811** (2017) 190003

15. L. Jian, X. Shali, Y. Qingguo, L. Lifeng, and W. Yufen, J. Quant. Spectr. Rad. Transfer **116** (2013) 41

16. O. Renner, E. Dalimier, E. Oks, F. Krasniqi, E. Dufour, R. Schott, and E. Foerster, J. Quant. Spectr. Rad. Transfer **99** (2006) 439

17. E. Oks, E. Dalimier, A.Ya. Faenov, T. Pikuz, Y. Fukuda, S. Jinno, H. Sakaki, H. Kotaki, A. Pirozhkov, Y. Hayashi, I. Skobelev, T. Kawachi, M. Kando, and K. Kondo, J. Phys. B: At. Mol. Opt. Phys. **47** (2014) 221001

18. E. Oks, E. Dalimier, A.Ya. Faenov, P. Angelo, S.A. Pikuz, E. Tubman, N.M.H. Butler, R.J. Dance, T.A. Pikuz, I.Yu. Skobelev, M.A. Alkhimova, N. Booth, J. Green, C. Gregory, A. Andreev, A. Zhidkov, R. Kodama, P. McKenna, and N. Woolsey, Optics Express **25** (2017) 1958

19. S. Depierreux, J. Fuchs, C. Labaune, A. Michard, H. A. Baldis, D. Pesme, S. Hüller, and G. Laval. Phys. Rev. Lett. **84**, 2869 (2000)

20. C.N. Danson, P.A. Brummitt, R.J. Clarke, J.L. Collier, B. Fell, A.J. Frackiewicz, S. Hawkes, C. Hernandez-Gomez, P. Holligan, M.H.R. Hutchinson, A. Kidd, W.J. Lester, I.O. Musgrave, D. Neely, D.R. Neville, P.A. Norreys, D.A. Pepler, C.J. Reason, W. Shaikh, T.B. Winstone, R.W.W. Wyatt, and B.E. Wyborn., Laser and Particle Beams, 23, 87 (2005)

21. NP Dover, CAJ Palmer, MJV Streeter, H. Ahmed, B. Albertazzi, M Borghesi,DC Carroll, J Fuchs, R. Heathcote, P Hilz, KF Kakolee, S Kar, R.Kodama, A. Kon, DA MacLellan, P McKenna, SR Nagel, D.Neely, MM Notley, M Nakatsutsumi ,R Prasad,G.Scott, M. Tampo, M. Zepf, J. Schreiber and Z Najmudin. New J. Phys. **18,** 013038 (2016)

22. A.Ya. Faenov S.A.Pikuz, A.I.Erko, B.A.Bryunetkin, V.M.Dyakin, G.V.Ivanenkov, A.R.Mingaleev, T.A.Pikuz, V.M.Romanova, T.A.Shelkovenko. Physica Scripta **50**, 333-338 (1994),

23. Ya.S. Lavrinenko, I.V. Morozov, S.A. Pikuz, I.Yu. Skobelev. J. Phys. CS **653,** 012027 (2015),

24. M.A. Alkhimova, S.A. Pikuz, A.Ya. Faenov, I.Yu. Skobelev J. Phys. CS 774, 012115 (2016))

25. J. Colgan, A.Ya. Faenov, S.A. Pikuz E. Tubman, N. M. H. Butler, J. Abdallah jr., R. J. Dance, T. A. Pikuz, I. Yu. Skobelev, M. A. Alkhimova, N. Booth, J. Green, C. Gregory, A. Andreev, R. Lötz, I. Uschmann, A. Zhidkov, R. Kodama, P. McKenna and N. Woolsey. Europhys. Letters **114** (2016) 35001

26. V.S. Lisitsa, Sov. Phys. Uspekhi **122** (1977) 603

27. W. L. Kruer, *The Physics of Laser Plasma Interactions* (Westview Press) 2003

28. P. Maine, D. Strickland, P. Bado, M. Pessot, and G. Mourou, IEEE J. Quantum Electron. **QE-24** (1988) 398

29. A. I. Akhiezer and R. V. Polovin, Sov. Phys. JETP **3** (1956) 696

30. W. Lünow, Plasma Phys. **10** (1968) 879

31. S. Guerin, P. Mora, J. C. Adam, A. Heron, and G. Laval, Phys. Plasmas **3** (1996) 2693

32. J. Fuchs, J.C. Adam, F. Amiranoff, S.D. Baton, P. Gallant, L. Gremillet, A. Heron, J.C. Kieffer, G. Laval, G. Malka, J.L. Miquel, P. Mora, N. Pepin, and C. Rousseaux, Phys. Rev. Lett. **80** (1998) 2326

33. A. Pukhov and J. Meyer-ter-Vehn, Phys. Rev.Lett. **79** (1997) 2686

34 A. Pukhov, Rep. Prog. Phys. **66** (2003) 47

35. G.A. Mourou, T. Tajima, and S.V. Bulanov, Rev. Modern Phys. **78** (2006) 309

36. P. Sauvan, E. Dalimier, E. Oks, O. Renner, S. Weber, and C. Riconda, J. Phys. B **42** (2009) 195001

37 E. Oks and G. V. Sholin, Sov. Phys. Tech. Phys. **21** (1976) 144

38. C. A. Iglesias, H. E. Dewitt, J. L. Lebowitz, D. MacGowan, and W.B. Hubbard, Phys. Rev. A **31** (1985) 1698

39. E. Dalimier and E. Oks, J.Phys. B: At. Mol. Opt. Phys. **50** (2017) 025701

40. S. Djurovic, M. Ćirišan, A.V. Demura, G.V. Demchenko, D. Nikolić, M.A. Gigosos, and M.A. González, Phys. Rev. E **79** (2009) 046402

41. A.V. Demura, G.V. Demchenko, and D. Nikolic, Europ. Phys. J. D **46** (2008) 111